Available online at www.sciencedirect.com
ScienceDirect
Journal of Power Sources 180 (2008) 71–83
JOURNAL OF POWER SOURCES
www.elsevier.com/locate/jpowsour

Non-isothermal dynamic modelling and optimization of a direct methanol fuel cell

DaeHo Ko [a,*], MinJeong Lee [a], Won-Hyouk Jang [a], Ulrike Krewer [b]

[a] *Samsung SDI Co., Ltd., CAE Team Kongse-dong, Giheung-gu, Yongin-si, Gyeonggi-do 446-577, Republic of Korea*
[b] *Samsung SDI Co., Ltd., Energy Laboratory, 575 Shin-dong, Yeongtong-gu, Suwon-si, Gyeonggi-do 443-391, Republic of Korea*

Received 11 October 2007; received in revised form 18 December 2007; accepted 29 January 2008
Available online 14 February 2008

Abstract

A non-isothermal dynamic optimization model of direct methanol fuel cells (DMFCs) is developed to predict their performance with an effective optimum-operating strategy. After investigating the sensitivities of the transient behaviour (the outlet temperature, crossovers of methanol and water, and cell voltage) to operating conditions (the inlet flow rates into anode and cathode compartments, and feed concentration) through dynamic simulations, we find that anode feed concentration has a significantly larger impact on methanol crossover, temperature, and cell voltage than the anode and cathode flow rates. Also, optimum transient conditions to satisfy the desired fuel efficiency are obtained by dynamic optimization. In the developed model, the significant influence of temperature on DMFC behaviour is described in detail with successful estimation of its model parameters.

Keywords: Direct methanol fuel cell; Dynamic simulation and optimization; Non-isothermal model; Optimum operation

1. Introduction

Direct methanol fuel cell (DMFC) systems are attractive for portable and stationary power applications. The fuel (methanol) is easy to store and deliver, and has a high specific energy. The design complexity of DMFC systems is reduced by eliminating the reforming units that are required to produce hydrogen for polymer electrolyte membrane fuel cells (PEMFCs). In view of designing the systems, there are two types of DMFCs, namely, passive-feed DMFCs and active DMFCs. Studies of passive DMFCs have been undertaken by Chen and Yang [1], Kim et al. [2], Liu et al. [3], Shimizu et al. [4], and Chen and Zhao [5]. Passive-feed DMFCs have advantages in eliminating parasitic power loss of pumps and fans because without an active (convective) feed supply, oxygen is supplied by air-breathing and methanol is diffused into the anode from the fuel cartridge driven by a concentration gradient. By contrast, active DMFCs can control the flow rate of the feed and air by means of pumps and/or fans to cope with the varying power loads and environmental conditions. However, both types of DMFCs still have low fuel efficiency and specific power compared with hydrogen fed PEMFCs due to mass crossover problems and slow methanol oxidation.

The fuel efficiency and the available oxygen concentration at the cathode catalyst sites are reduced by methanol crossover through which a large amount of methanol is transported from the anode to the cathode catalyst layer. Oxygen transport to the catalyst layer is also prevented as water at the anode crosses the membrane. To solve these problems, much research has been conducted. In modelling work, Simoglou et al. [6,7] have described an experimental study of the dynamics of a DMFC and have developed an empirical model of the cell voltage dynamics with a feasibility study of model-based scale-up and scale-down.

Dohle et al. [8] examined the heat and power management of a DMFC system, and in particular investigated the influence of water vaporization in the cathode on the heat management of the DMFC system. Dohle and Wippermann [9] developed a semi-empirical model to predict methanol permeation, overpotentials, and polarization curves. Sundmacher et al. [10] formulated a dynamic lumped parameter DMFC model by deriving anode kinetics consisting of a four-step reaction mechanism. Krewer

* Corresponding author. Tel.: +82 41 520 6271; fax: +82 41 520 6655.
E-mail addresses: daeho.ko@samsung.com, daehoko@hotmail.com (D. Ko).

0378-7753/$ – see front matter © 2008 Elsevier B.V. All rights reserved.
doi:10.1016/j.jpowsour.2008.01.083

Nomenclature

A^{s} cross-sectional active electrode area (1.0×10^{-3} m^2)
B constant depending on the fuel cell and its operating state (V)
C concentration (mol m^{-3})
C_{feed} feed concentration (mol m^{-3})
C_i^{CL} concentration of component i in catalyst layer (mol m^{-3})
C_a double layer capacity of anode (F m^{-2})
C_c double layer capacity of cathode (F m^{-2})
$C_{c,loss}$ concentration loss of cathode part (V)
C_i^{F} feed concentration of component i (mol m^{-3})
$C_{p,solid}$ heat capacity of cell (J kg^{-1} K^{-1})
$C_{pa,i}^{out}$ heat capacity of outlet stream from anode part (J mol^{-1} K^{-1})
$C_{pc,i}^{out}$ heat capacity of outlet stream from cathode part (J mol^{-1} K^{-1})
d^{M} PEM thickness (2.0×10^{-4} m)
$D_{CH_3OH}^{M}$ Diffusion coefficient of methanol in membrane (2.9×10^{-10} m^2 s^{-1})
F Faraday constant (96,485 C mol^{-1})
$h_{a,i}^{in}$ inlet enthalpy into anode part (J mol^{-1})
$h_{c,i}^{in}$ inlet enthalpy into cathode part (J mol^{-1})
$h_{a,i}^{out}$ outlet enthalpy from anode part (J mol^{-1})
$h_{c,i}^{out}$ outlet enthalpy from cathode part (J mol^{-1})
i_{cell} cell current density (A m^{-2})
$i_{crossover}$ crossover cell current density (A m^{-2})
i_{lim} limiting current density (A m^{-2})
k_j rate constant of reaction j (mol m^{-2} s^{-1})
k^{LS} mass transfer coefficient (m s^{-1})
k_p hydraulic permeability of membrane (1.57×10^{-18} m^2)
K_j equilibrium constant of reaction j
m_{solid} cell mass (kg)
Mw_{water} molecular weight of water (kg mol^{-1})
n_a mole amount of anode part (mol)
n_c mole amount of cathode part (mol)
$n_{CH_3OH}^{M}$ methanol crossover (mol m^{-2} s^{-1})
$\dot{n}_a^{in}$ inlet molar flow rate into anode part (mol s^{-1})
$\dot{n}_c^{in}$ inlet molar flow rate into cathode part (mol s^{-1})
n_d electro-osmotic drag coefficient
n_{water}^{M} water crossover (mol m^{-2} s^{-1})
P_a total pressure of anode part (Pa)
P_c total pressure of cathode part (Pa)
P_{O_2} partial pressure of oxygen into cathode part (Pa)
P_{STD} standard pressure of (1.013×10^5 Pa)
$Power_{cell}$ power generation from DMFC cell (J s^{-1})
$Power_{comp}$ compressor power consumption (J s^{-1})
$Power_{Net}$ net power generation from DMFC system (J s^{-1})
$Q_{a,rxn}$ reaction heat of anode catalyst layer (J s^{-1})
$Q_{c,rxn}$ reaction heat of cathode catalyst layer (J s^{-1})
$Q_{MeOHXover}$ reaction heat of methanol oxidation resulting from methanol crossover (J mol^{-1})
Q_{loss} heat loss of cell resulting from convection, conduction, radiation, and any others (J s^{-1}) (assumed to be zero in this work due to adiabatic condition)
r reaction rate (mol m^{-2} s^{-1})
R universal gas constant (8.314 J mol^{-1} K^{-1})
RME relative mean error (%)
t time (s)
$t_{initial}$ start time of the operation (s)
t_{final} end time of the operation (s)
T cell temperature (K)
$\dot{V}_a^{in}$ inlet flow rate into the anode part (m^3 s^{-1})
$\dot{V}_c^{in}$ inlet flow rate into the cathode part (m^3 s^{-1})
V_{cell} cell voltage (V)
V_{cell}^{0} open circuit voltage of cell (V)
$x_{a,i}^{out}$ outlet mole fraction from anode part
$x_{c,i}^{out}$ outlet mole fraction from cathode part

Greek symbols
α charge transfer coefficient (0.5)
γ ratio of heat capacity, *i.e.*, heat capacity at constant pressure divided by that at constant volume (1.4)
η_a anode electrode overpotential (V)
η_c cathode electrode overpotential (V)
η_{Fuel} fuel efficiency
Θ_i surface fraction covered by component i
κ^{M} conductivity of membrane (17 Ω^{-1} m^{-1})
μ pore fluid viscosity in membrane (3.353×10^{-4} kg m^{-1} s^{-1})
ρ_{water} water density (kg m^{-3})
τ mean residence tim in the anode or cathode compartment (s)

Subscripts
a anode
c cathode
feed methanol inlet into the anode
Pt free active sites of platinum catalyst
Pt_3–COH Pt_3–COH occupied platinum sites
Pt–COOH Pt–COOH occupied platinum sites
Ru free active sites of ruthenium catalyst
Ru–OH Ru–OH occupied ruthenium sites

Superscripts
CL catalyst layer
LS from liquid bulk to surface
M membrane (PEM)
θ at standard conditions

et al. [11] presented the dynamic behaviour of DMFCs through a dynamic model with an updated reaction mechanism. Schultz and Sundmacher [12] simulated a one-dimensional, rigorous, mathematical model of a DMFC with focus on a realistic description of mass and energy transport, as well as the physical properties of the PEM material.

Through the application of computational fluid dynamics (CFDs), Cheng et al. [13] derived a simplified CFD model to predict fuel cell performance on personal computers without huge computation time. A 3-D CFD model was also created by Kjeang et al. [14] to analyze methanol transport in a flowing-electrolyte DMFC.

Apart from the above simulation work, including CFD modelling and differential algebraic equation (DAE) modelling, Xu et al. [15] performed optimization of the isothermal DMFC DAE model based on the study by Sundmacher et al. [10].

In addition to the active research on DMFC modelling and the strong influence of membrane–electrode assembly (MEA) temperature on DMFC performance, an optimization study of a non-isothermal DMFC, which involves the flow rates and the reaction enthalpies of inlet and outlet streams, is necessary to determine an optimum-operating condition. Thus, the work reported here presents the development of a non-isothermal dynamic DMFC model by adding an energy balance to the isothermal model of Sundmacher et al. [10], together with dynamic simulations and optimization of the model. The next section introduces a non-isothermal differential algebraic equation model, updated from the isothermal model of Sundmacher et al. [10], and parameter estimation results. The dynamic behaviour of DMFC operation, *i.e.*, the effects of operating variables, and a dynamic optimization are discussed in the following sections.

2. Non-isothermal dynamic model of DMFC

2.1. Differential algebraic equation (DAE) model of DMFC

The basic structure of a DMFC reaction scheme is shown in Fig. 1, and the following total electrochemical reactions take place on the catalyst layers of the MEA.

$$\text{Anode}: CH_3OH(l) + H_2O(l) \xrightarrow{Pt/Ru} CO_2 + 6H^+ + 6e^-$$

$$V^{\theta,25\,^\circ C}_{CH_3OH \leftrightarrow CO_2} = 0.02\,V$$

$$\text{Cathode}: \frac{3}{2}O_2(g) + 6H^+ + 6e^- \xrightarrow{Pt} 3H_2O(l)$$

$$V^{\theta,25^\circ C}_{O_2 \leftrightarrow H_2O} = 1.23\,V$$

$$\text{Overall}: CH_3OH(l) + \frac{3}{2}O_2(g) \rightarrow CO_2(g) + 2H_2O(l)$$

$$V^{\theta,25^\circ C}_{Cell} = 1.21\,V$$

The summarized DAE model of Sundmacher et al. [10] is listed in the Table 1. The energy balance Eq. (13), described in more detail in the Appendix A, includes the moles of each component (liquid and gas phase) in the anode and cathode parts, the molar flow rates of the inlet and outlet streams of the cell, the mass and heat capacity of the solid state (the single-cell stack), the reaction heat of methanol oxidation due to methanol crossover, and the electrochemical reaction heats of anode and cathode catalyst layers.

$$\frac{dT}{dt} = \frac{\left[\sum_i \dot{n}^{in}_c x^{in}_{c,i}(h^{in}_{c,i} - h^{out}_{c,i}) + \sum_i \dot{n}^{in}_a x^{in}_{a,i}(h^{in}_{a,i} - h^{out}_{a,i}) - Q_{c,rxn} - Q_{a,rxn} - Q_{MeOHXover} n^M_{CH_3OH} A^S - Power_{cell} - Q_{loss}\right]}{m_{solid} C_{psolid} + n_c \sum_i (x^{out}_{c,i} C^{out}_{pc,i}) + n_a \sum_i (x^{out}_{a,i} C^{out}_{pa,i})} \quad (13)$$

Based on the energy balance the outlet temperature from the DMFC can be predicted, under given conditions of the inlet temperatures, molar flow rates and feed concentration, by adopting some of the assumptions made by Sundmacher et al. [10], namely:

- the compartment channels and catalyst layers are treated as continuous stirred tank reactors (CSTR), *i.e.*, a lumped MEA model
- ohmic drops in current-collectors and electric connections are negligible
- mass-transport resistances in the catalyst layers are negligible because the catalyst layers are very thin (*i.e.*, 10 μm) compared with that of the PEM (*i.e.*, 200 μm)
- mass-transport coefficients of the components (water and methanol) in the diffusion layer are equal
- the electrochemical oxidation of methanol at the anode follows the reaction mechanism given in Table 1 with the first step, Eq. (1), as a rate-determining step.

Also, the additional assumptions are made:

- there is no heat loss in the stack (adiabatic condition), that is, $Q_{loss} = 0$
- the electro-osmotic drag coefficient (n_d) is a function of the temperature ($n_d = -5.77 + 0.027\ T$); this linear equation is obtained by fitting the data of Ren and Gottesfeld [16]
- the inlet flow rate into the anode or the cathode is the same as the respective outlet flow rate based on the lumped MEA model assumption.

Water crossover is derived from the paper of Lu et al. [17], *i.e.*,

$$n^M_{water} = (n_d + 0.5)\left(\frac{i_{cell}}{F}\right) - \frac{k_p}{\mu}(P_c - P_a)\frac{\rho_{water}}{M w_{water}} \quad (14)$$

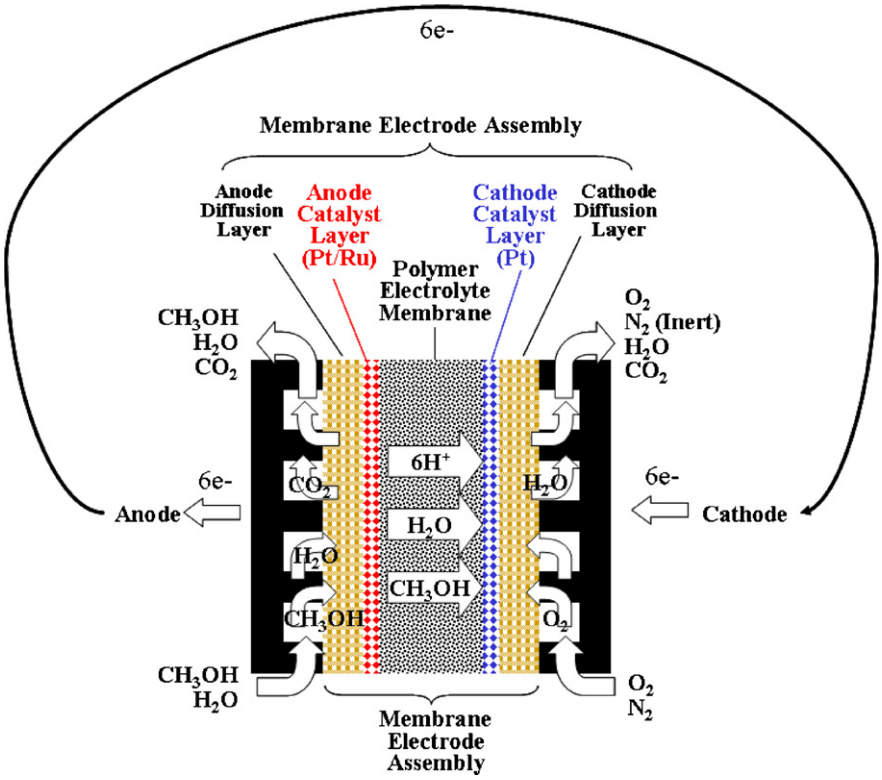

Fig. 1. Structure and reaction scheme of DMFC.

Table 1
DAE model taken from Sundmacher et al. [10]

Electrode reaction rate expressions

Anode

$$r_1 = k_1 \exp\left(\frac{\alpha_1 F}{RT}\eta_a\right)\left\{\Theta_{Pt}^3 C_{CH_3OH}^{CL} - \frac{1}{K_1}\exp\left(-\frac{F}{RT}\eta_a\right)\Theta_{Pt_3-COH}\right\} \quad (1)$$

$$r_2 = k_2 \exp\left(\frac{\alpha_2 F}{RT}\eta_a\right)\left\{\Theta_{Ru} - \frac{1}{K_2}\exp\left(-\frac{F}{RT}\eta_a\right)\Theta_{Ru-OH}\right\} \quad (2)$$

$$r_3 = k_3\left\{\Theta_{Pt_3-COH}\Theta_{Ru-OH}^2 - \frac{1}{K_3}\Theta_{Pt-COOH}\Theta_{Pt}^2\Theta_{Ru}^2\right\} \quad (3)$$

$$r_4 = k_4\left\{\Theta_{Pt-COOH}\Theta_{Ru-OH} - \frac{1}{K_4}C_{CO_2}^{CL}\Theta_{Pt}\Theta_{Ru}\right\} \quad (4)$$

Cathode

$$r_5 = k_5 \exp\left(\frac{\alpha_5 F}{RT}\eta_c\right)\left\{1 - \exp\left(-\frac{F}{RT}\eta_c\right)\left(\frac{P_{O_2}}{P_c}\right)^{3/2}\right\} \quad (5)$$

Mass balances of anode compartment

$$\frac{dC_{CH_3OH}}{dt} = \frac{C_{CH_3OH}^F - C_{CH_3OH}}{\tau_a} - \frac{k^{LS}A^S}{V_a}(C_{CH_3OH} - C_{CH_3OH}^{CL}) \quad (6)$$

$$\frac{dC_{CO_2}}{dt} = \frac{C_{CO_2}^F - C_{CO_2}}{\tau_a} - \frac{k^{LS}A^S}{V_a}(C_{CO_2} - C_{CO_2}^{CL}) \quad (7)$$

Mass balances of catalyst layer

$$\frac{dC_{CH_3OH}^{CL}}{dt} = \frac{k^{LS}A^S}{V_a^{CL}}(C_{CH_3OH} - C_{CH_3OH}^{CL}) - \frac{A^S}{V_a^{CL}}n_{CH_3OH}^M - \frac{A^S}{V_a^{CL}}r_1 \quad (8)$$

$$\frac{dC_{CO_2}^{CL}}{dt} = \frac{k^{LS}A^S}{V_a^{CL}}(C_{CO_2} - C_{CO_2}^{CL}) + \frac{A^S}{V_a^{CL}}r_1 \quad (9)$$

Charge balances

$$\frac{\partial\eta_a}{\partial t} = \frac{i_{cell} - 6Fr_1}{C_a} \quad (10)$$

$$\frac{\partial\eta_c}{\partial t} = \frac{-i_{cell} - 6F(r_5 + n_{a,CH_3OH}^M)}{C_c} \quad (11)$$

The methanol crossover

$$n_{CH_3OH}^M = \left(\frac{D_{CH_3OH}^M C_{a,CH_3OH}^{CL}}{d_M}\right)(Pe)\left(\frac{\exp(Pe)}{\exp(Pe)-1}\right) \text{ here, } \quad Pe \equiv v\frac{d^M}{D_{CH_3OH}^M} \quad (12)$$

where k_p is the hydraulic permeability of a membrane; μ is the pore fluid viscosity in the membrane; ρ_{water} is the water density; Mw_{water} is the molecular weight of water.

Since the cathode overpotential does not contain concentration loss whereas the anode overpotential does, the concentration loss at the cathode is given by [18]:

$$C_{c,loss} = B \ln\left(1 - \frac{i_{cell}}{i_{lim}}\right) \quad (15)$$

where B is a constant depending on the fuel cell and the operating state [18].

The overall cell voltage is modified from that of the paper [10], *i.e.*,

$$V_{cell} = V_{cell}^0 - \eta_a + \eta_c - \frac{d^M}{\kappa^M} i_{cell} + B \ln\left(1 - \frac{i_{cell}}{i_{lim}}\right) \quad (16)$$

2.2. Optimization strategy

Based on the DAE model in Section 2.1, parameter estimation, dynamic simulation and optimization were performed by using the gPROMS modelling tool [19]. For the dynamic simulation, a DASOLV code, one of the standard differential algebraic solvers in the gPROMS, was employed with a dynamic optimization solver, DYNOPT, for the optimization and parameter estimation.

The DASOLV solver, based on a variable time step and variable order backward differentiation formulae (BDF), is applicable for a wide range of problems due to its efficient treatment of large and sparse systems of equations that include the variable within the lower and upper bounds except highly oscillatory behaviour models with frequent discontinuities, It provides strong advantages in automatically adjusting each time step and in yielding efficient finite difference approximations.

A CVP_SS solver of the DYNOPT, adopted for the optimization, is based on a control vector parameterization (CVP) approach assuming that the time-varying control variables are piecewise constant (or piecewise linear) functions of time over a specified number of control intervals.

The CVP_SS solver employs a single-shooting dynamic optimization algorithm, that:

(i) chooses the duration of each control interval and the values of the control variables
(ii) solves a dynamic system model over the entire time horizon by starting from the initial time point
(iii) determines the values of the optimized objective function to satisfy the constraints
(iv) repeats the procedure until convergence to the optimum is reached.

The non-linear programming (NLP) solver of the CVP_SS is a SRQPD solver which employs a sequential quadratic programming (SQP) approach.

Table 2
Reference values of kinetic parameters

Parameters	Reference values
$k_1 = k_{1,ref}$	1.0×10^{-7}
$k_2 = k_{2,ref}$	1
$k_3 = k_{3,ref}$	0.01
$k_4 = k_{4,ref}$	1
$k_5 = k_{5,ref}$	7.0×10^{-5}
$K_1 = K_{1,ref}$	1
$K_2 = K_{2,ref}$	0.02
$K_3 = K_{3,ref}$	1
$K_4 = K_{4,ref}$	0.02

2.3. Parameter estimation

The parameters to be estimated are selected from the chemical reaction parameters, *i.e.*, $k_1, k_2, k_3, k_4, k_5, K_1, K_2, K_3$, and K_4 in the Eqs. (1)–(5) of Table 1. The three parameters (k_2, k_3, and k_4) are screened in advance because they have no influence on the DMFC behaviour in the current model, *i.e.*, $r_2 = r_3 = r_4 \approx 0$ based on the chemical equilibrium assumption and allow calculation of the surface fraction of catalyst areas [10]. Then, the sensitivities of the remaining parameters (k_1, k_5, K_1, K_2, K_3, and K_4) to the cell voltage are analyzed to choose those for estimation by using the reference values in Table 2. In Table 3, V_J is the voltage when the chemical reaction parameter is J, with $J \in \{k_{1,ref}, k_{5,ref}, K_{1,ref}, \ldots, K_{4,ref}\}$. $V_{J\times 0.5}$ and $V_{J\times 1.5}$ are the voltages when the corresponding parameter value is multiplied by 0.5 and 1.5, respectively.

Since the cell voltage is mainly affected by four kinetic parameters (k_1, k_5, K_2, and K_4), as shown in Table 3, these parameters are finally selected as decision variables for the estimation.

The constant (B) and limiting current density (i_{lim}) in the cathode concentration loss term are also treated as parameters for estimation. The optimization model for the parameter estimation is formulated as:

$$\text{MIN} \cdot f = \frac{1}{30}\left(\sum_{k=1}^{30}\left|\frac{V_{cell}^{Cal}(i_{cell}^k) - V_{cell}^{Exp}(i_{cell}^k)}{V_{cell}^{Exp}(i_{cell}^k)}\right|\right) + \frac{1}{3}\left(\sum_{l=1}^{3}\left|\frac{\eta_a^{Cal}(i_{cell}^l) - \eta_a^{Exp}(i_{cell}^l)}{\eta_a^{Exp}(i_{cell}^l)}\right|\right) \quad (17)$$

Table 3
Sensitivity analysis of kinetic parameters to voltage ($i_{cell} = 2000\ A\ m^{-2}$)

Parameters	Voltage deviation [%] when $J = k_{1,ref}$, ..., $k_{5,ref}$, $K_{1,ref}$, ..., or $K_{4,ref}$	
	$\left\lvert\frac{V_{J\times 0.5} - V_J}{V_J}\right\rvert \times 100$	$\left\lvert\frac{V_{J\times 1.5} - V_J}{V_J}\right\rvert \times 100$
$J = k_1$	2.58	1.39
$J = k_5$	10.73	6.28
$J = K_1$	~0.00	~0.00
$J = K_2$	4.18	2.41
$J = K_3$	~0.00	~0.00
$J = K_4$	4.18	2.41

Table 4
Initial guess values for parameter estimation

Parameters	Reference values
k_1	1.0×10^{-7} (mol m^{-2} s^{-1})
k_5	7.0×10^{-5} (mol m^{-2} s^{-1})
K_2	0.02
K_4	0.02
B	0.01 (V)
i_{lim}	7000 (A m^{-2})

Subject to:

$$10^{-4}\,\text{V} \le B \le 1\,\text{V}$$

$$6000\,\text{A m}^{-2} \le i_{\text{lim}} \le 10,000\,\text{A m}^{-2}$$

$$1.0 \times 10^{-9}\,\text{mol m}^{-2}\,\text{s}^{-1} \le k_1 \le 1.0 \times 10^{-5}\,\text{mol m}^{-2}\,\text{s}^{-1}$$

$$1.0 \times 10^{-10}\,\text{mol m}^{-2}\,\text{s}^{-1} \le k_5 \le 1.0 \times 10^{-4}\,\text{mol m}^{-2}\,\text{s}^{-1}$$

$$1.0 \times 10^{-4} \le K_2 \le 5.0$$

$$1.0 \times 10^{-4} \le K_4 \le 5.0$$

$$\text{RME}_{V_{\text{cell}}} = \frac{1}{30}\left(\sum_{k=1}^{30}\left|\frac{V_{\text{cell}}^{\text{Cal}}(i_{\text{cell}}^k) - V_{\text{cell}}^{\text{Exp}}(i_{\text{cell}}^k)}{V_{\text{cell}}^{\text{Exp}}(i_{\text{cell}}^k)}\right|\right) \le 5\%$$

$$\text{RME}_{\eta_{\text{A}}} = \frac{1}{3}\left(\sum_{l=1}^{3}\left|\frac{\eta_{\text{a}}^{\text{Cal}}(i_{\text{cell}}^l) - \eta_{\text{a}}^{\text{Exp}}(i_{\text{cell}}^l)}{\eta_{\text{a}}^{\text{Exp}}(i_{\text{cell}}^l)}\right|\right) \le 5\%$$

Model Eqs. (1)–(16), optimization tolerance = 10^{-6}.

The initial guess values for this parameter estimation are shown in Table 4.

In Eq. (17) f is an objective function to be minimized; B is a constant that depends on the fuel cell and its operating state [18]; i_{lim} is the limiting current density; i_{cell}^k and i_{cell}^l are the current densities of the k-th and l-th cell, respectively; $V_{\text{cell}}^{\text{Cal}}(i_{\text{cell}}^k)$ and $V_{\text{cell}}^{\text{Exp}}(i_{\text{cell}}^k)$ are the calculated and measured cell voltage, respectively, when the curent density is i_{cell}^k; $\eta_{\text{a}}^{\text{Cal}}(i_{\text{cell}}^l)$ and $\eta_{\text{a}}^{\text{Exp}}(i_{\text{cell}}^l)$ are the calculated and measured overpotential of the anode, respectively, when the current density is $i_{\text{cell}}^{\text{l}}$. The measured number of data points for cell voltage is thirty and that for anode overpotential is three.

The estimated values of the parameters are listed in Table 5. The relative mean errors (RMEs) of the cell voltage and anode overpotential are calculated by Eqs. (18) and (19).

Table 5
Estimated values for parameters

Parameters	Reference values
k_1	1.76×10^{-7} [mol m^{-2} s^{-1}]
k_5	1.00×10^{-4} [mol m^{-2} s^{-1}]
K_2	3.45×10^{-2}
K_4	3.45×10^{-2}
B	1.00×10^{-4} [V]
i_{lim}	7034.84 [A m^{-2}]

Total CPU time for calculation: 552.94 s on Pentium 4 with 3 GHz CPU and 512 MB RAM, number of NLP iterations: 8.

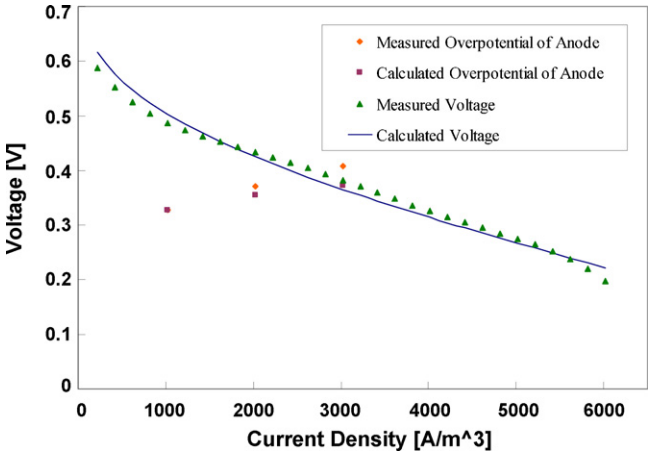

Fig. 2. Parameter estimation results: cell voltage and anode overpotential vs. current density (cell temperature = 343.15 K).

$$\text{RME}_{V_{\text{Cell}}} = \frac{1}{30}\left(\sum_{k=1}^{30}\left|\frac{V_{\text{cell}}^{\text{Cal}}(i_{\text{cell}}^k) - V_{\text{cell}}^{\text{Exp}}(i_{\text{cell}}^k)}{V_{\text{cell}}^{\text{Exp}}(i_{\text{cell}}^k)}\right|\right) = 3.51\% \tag{18}$$

$$\text{RME}_{\eta_{\text{a}}} = \frac{1}{3}\left(\sum_{l=1}^{3}\left|\frac{\eta_{\text{cell}}^{\text{Cal}}(i_{\text{cell}}^l) - \eta_{\text{cell}}^{\text{Exp}}(i_{\text{cell}}^l)}{\eta_{\text{cell}}^{\text{Exp}}(i_{\text{cell}}^l)}\right|\right) = 4.40\% \tag{19}$$

Because the RMEs are reasonably small and the simulated data are in good agreement with the measured data, as shown in Fig. 2, the estimated values of the model parameters describe the steady-state performance of the DMFC well.

3. Dynamic behaviour of DMFC

The effect of the operating variables (feed concentration, anode flow rate, and cathode flow rate) on the temperature, crossovers and voltage was checked using the obtained parameter values, when the current density is 2000 A m^{-2}. The feed concentration has an influence on the cell voltage, temperature and crossovers of methanol and water, as shown in Figs. 3–6. The temperature increases as the feed concentration increases (Fig. 3) because the higher feed concentration leads to higher methanol crossover (Fig. 4). The methanol crossover also influences the methanol oxidation reaction, which is exothermic. The feed concentration affects the water crossover too, as shown in Fig. 5, due to its effect on the system temperature. The cell voltage decreases as the feed concentration increases at 2000 A m^{-2} (Fig. 6) due to the strong influence of crossover on the cathodic overpotential.

As shown in Fig. 7, higher flow rate of feed lowers the cell temperature at constant feed concentration (1 M). This means the feed acts as a coolant. Methanol crossover decreases as the flow rate decreases since the amount of methanol supplied is reduced (Fig. 8). Due to the effect of temperature on the water drag coefficient, water crossover increases as the flow rate of feed decreases (Fig. 9). The cell voltage changes proportionally to the flow rate (Fig. 10).

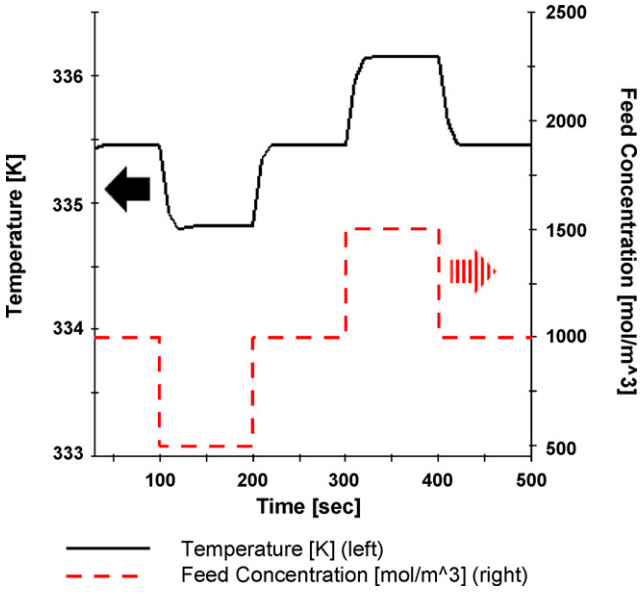

Fig. 3. Temperature profile vs. feed concentration at non-isothermal conditions (initial temperature = 25 °C, current density = 2000 A m^{-2}, anode inlet temperature = 333.15 K, cathode inlet temperature = 298.15 K).

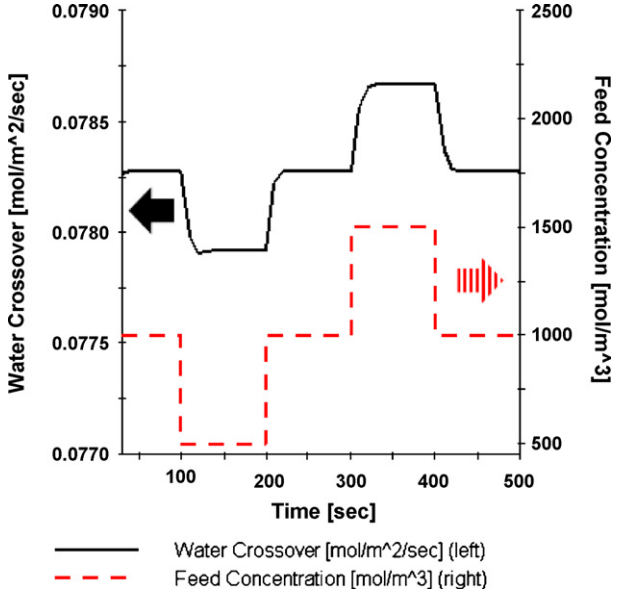

Fig. 5. Water crossover profile vs. feed concentration (initial temperature = 25 °C, current density = 2000 A m^{-2}, anode inlet temperature = 333.15 K, cathode inlet temperature = 298.15 K).

As the air flow rate increases, the temperature decreases because air also affects as a coolant (Fig. 11). The crossovers of methanol and water decrease when the air flow rate increases, as demonstrated in Figs. 12 and 13. The data in Fig. 14 show that a higher air flow rate results in a higher cell voltage.

4. Dynamic optimization of DMFC

A dynamic optimization of the DMFC was performed to achieve the desired fuel efficiency, 80%, and to satisfy the varying power load. The decision variables are the operating conditions such as inlet flow rates into the anode and the cathode, as well as the feed concentration. Fig. 15 shows the assumed change in power density load. The optimization model is formulated as follows:

$$\text{MIN} \cdot f = \left| \frac{\eta_{\text{Fuel,ave}}^{\text{Cal}} - \eta_{\text{Fuel}}^{\text{Desired}}}{\eta_{\text{Fuel}}^{\text{Desired}}} \right| \tag{20}$$

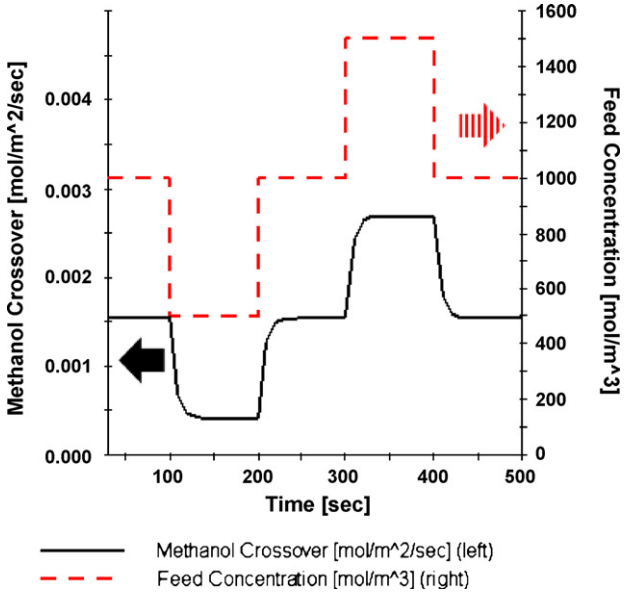

Fig. 4. Methanol crossover profile vs. feed concentration (initial temperature = 25 °C, current density = 2000 A m^{-2}, anode inlet temperature = 333.15 K, cathode inlet temperature = 298.15 K).

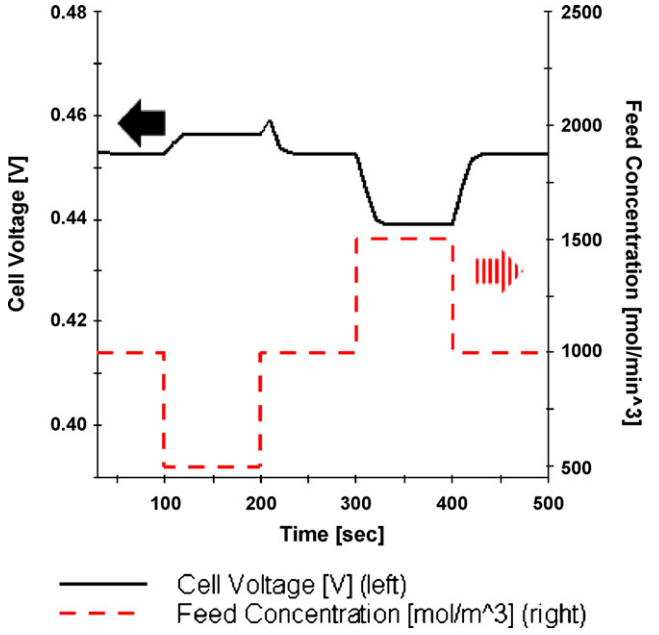

Fig. 6. Cell voltage profile vs. feed concentration (initial temperature = 25 °C, current density = 2000 A m^{-2}, anode inlet temperature = 333.15 K, cathode inlet temperature = 298.15 K).

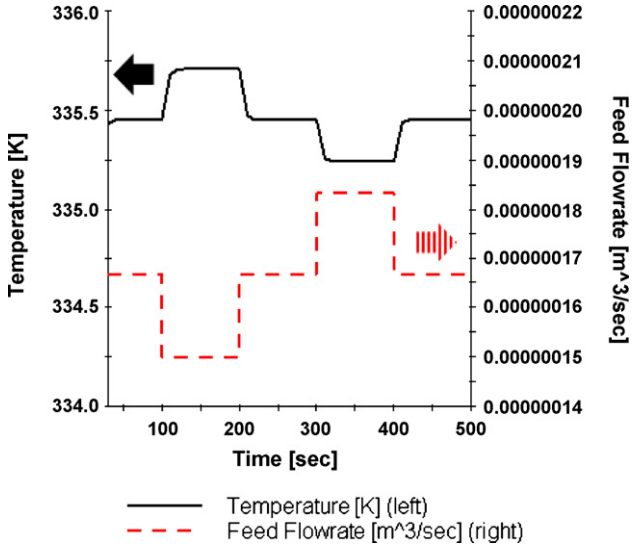

Fig. 7. Temperature profile vs. feed flow rate at non-isothermal condition (initial temperature = 25 °C, current density = 2000 A m^{-2}, anode inlet temperature = 333.15 K, cathode inlet temperature = 298.15 K).

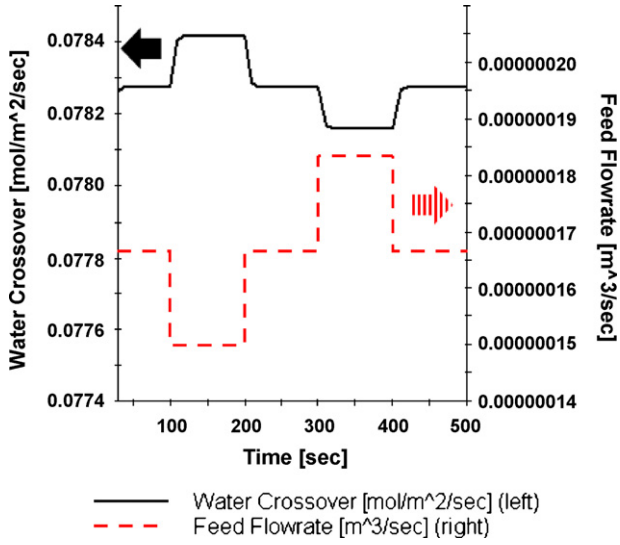

Fig. 9. Water crossover profile vs. feed flow rate (initial temperature = 25 °C, current density = 2000 A m^{-2}, anode inlet temperature = 333.15 K, cathode inlet temperature = 298.15 K).

Subject to:

$$1.0 \times 10^{-8} \le \dot{V}_a^{in} \le 1.0 \times 10^{-5}\ m^3\ s^{-1}$$
$$1.0 \times 10^{-7} \le \dot{V}_c^{in} \le 1.0 \times 10^{-4}\ m^3\ s^{-1}$$
$$900 \le C_{feed} \le 1100\ mol\ m^{-3}$$

Model Eqs. (1)–(26), optimization tolerance = 10^{-3}.Here,

$$i_{crossover} = (6F)(n^{M}_{CH_3OH}) \quad (21)$$

$$\eta^{Cal}_{Fuel} = \frac{i_{cell}}{i_{cell} + i_{crossover}} \quad (22)$$

$$\eta^{Cal}_{Fuel,ave} = \frac{\int_{t_{initial}}^{t_{final}} \eta^{Cal}_{Fuel} dt}{t_{final} - t_{initial}} \quad (23)$$

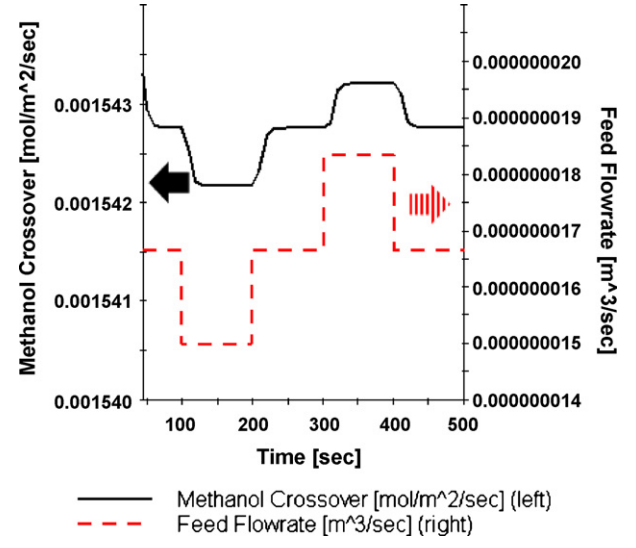

Fig. 8. Methanol crossover profile vs. feed flow rate (initial temperature = 25 °C, current density = 2000 A m^{-2}, anode inlet temperature = 333.15 K, cathode inlet temperature = 298.15 K).

where η^{Cal}_{Fuel} is the calculated fuel efficiency; $\eta^{Cal}_{Fuel,ave}$ is the average calculated fuel efficiency; $\eta^{Desired}_{Fuel}$ is the desired fuel efficiency; $i_{crossover}$ is the crossover current density; t_{final} is the end time of the operation; $t_{initial}$ is the start time of the operation (=0 s). The power equations are described by Eqs. (24)–(26). The compressor power consumption ($Power_{comp}$), assumed as an adiabatic condition, is given by Eq. (24) [20].

$$Power_{comp} = \left\{\frac{371 T_c^{in} \gamma \dot{V}_c^{in}}{(\gamma - 1)\eta_{comp,eff}}\right\}\left\{\left(\frac{P_c}{P_{STD}}\right)^{(1-(1/\gamma))} - 1\right\} \quad (24)$$

where γ is the ratio of heat capacity, *i.e.*, the heat capacity at constant pressure divided by that at constant volume (=1.4); T_c^{in} is the inlet temperature into the cathode ; $\dot{V}_c^{in}$ is the inlet flow rate into the cathode; $\eta_{comp,eff}$ is compressor efficiency

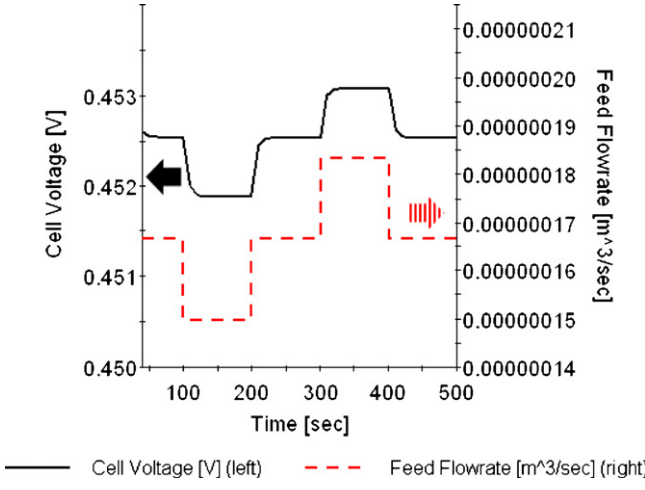

Fig. 10. Cell voltage profile vs. feed flow rate (initial temperature = 25 °C, current density = 2000 A m^{-2}, anode inlet temperature = 333.15 K, cathode inlet temperature = 298.15 K).

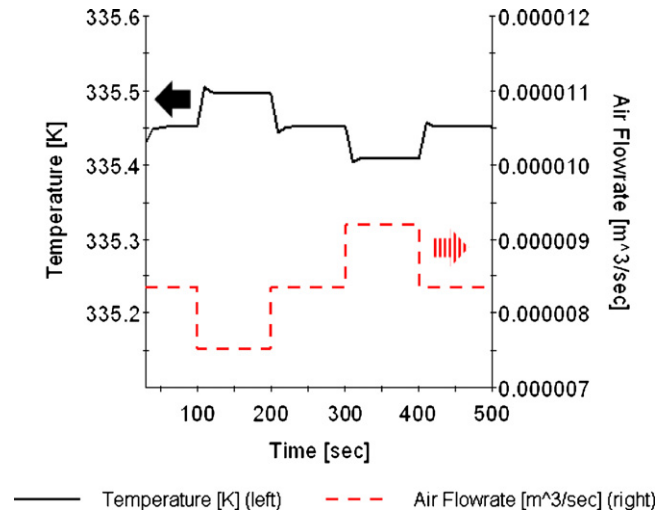

Fig. 11. Temperature profile vs. air flow rate at non-isothermal condition (initial temperature = 25 °C, current density = 2000 A m^{-2}, anode inlet temperature = 333.15 K, cathode inlet temperature = 298.15 K).

(=80%); P_c is total pressure at the cathode; P_{STD} is the standard pressure.

The power generation of the DMFC cell ($Power_{cell}$) is calculated by:

$$Power_{cell} = i_{cell} \times V_{cell} \times A^S \quad (25)$$

Thus, the net power generation from the DMFC system ($Power_{Net}$) is obtained by Eq. (26), and it must be the same as the required power load.

$$Power_{Net} = Power_{cell} - Power_{comp} \quad (26)$$

The initial guess values for the optimization are listed in Table 6. The optimum dynamic operating conditions of the feed and air flow rates, and feed concentration are given in Figs. 16–18, respectively. The data show that the decision vari-

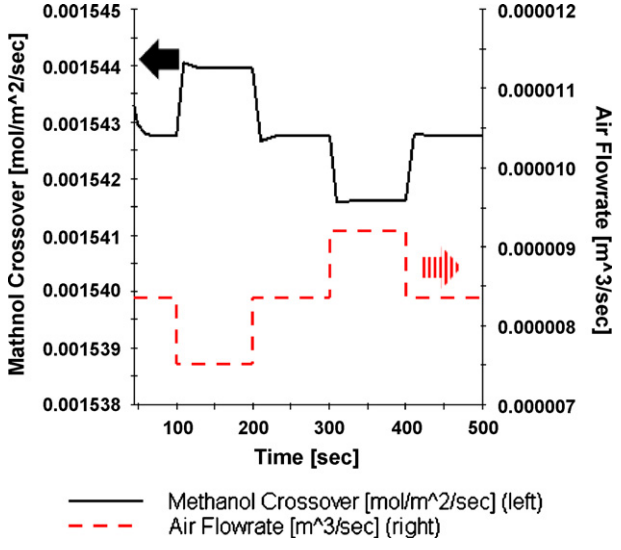

Fig. 12. Methanol crossover profile vs. air flow rate (initial temperature = 25 °C, current density = 2000 A m^{-2}, anode inlet temperature = 333.15 K, cathode inlet temperature = 298.15 K).

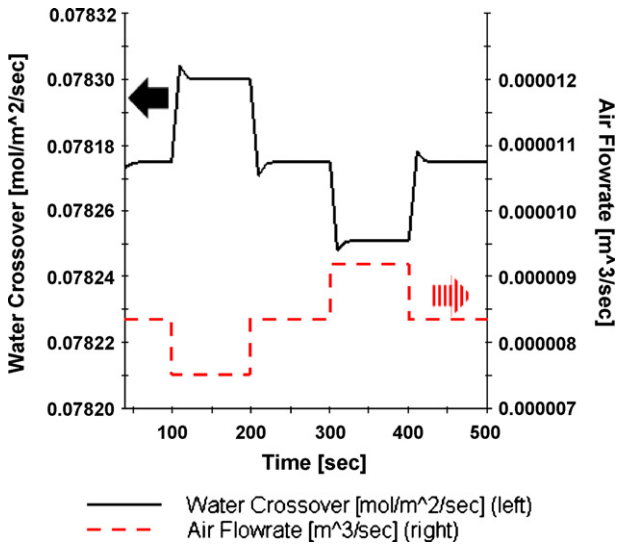

Fig. 13. Water crossover profile vs. air flow rate (initial temperature = 25 °C, current density = 2000 A m^{-2}, anode inlet temperature = 333.15 K, cathode inlet temperature = 298.15 K).

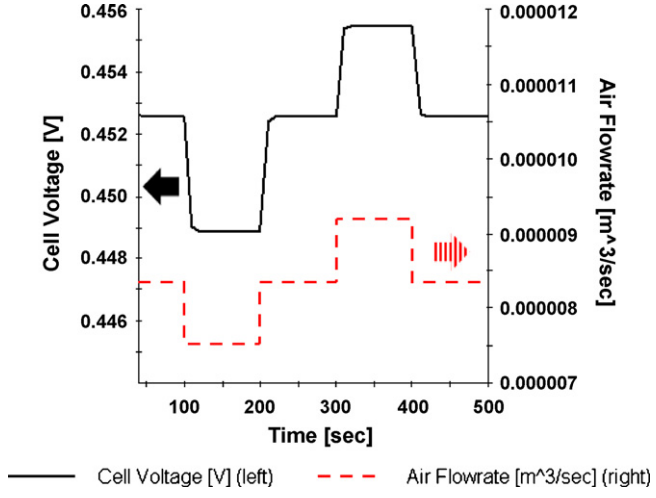

Fig. 14. Cell voltage profile vs. air flow rate (initial temperature = 25 °C, current density = 2000 A m^{-2}, anode inlet temperature = 333.15 K, cathode inlet temperature = 298.15 K).

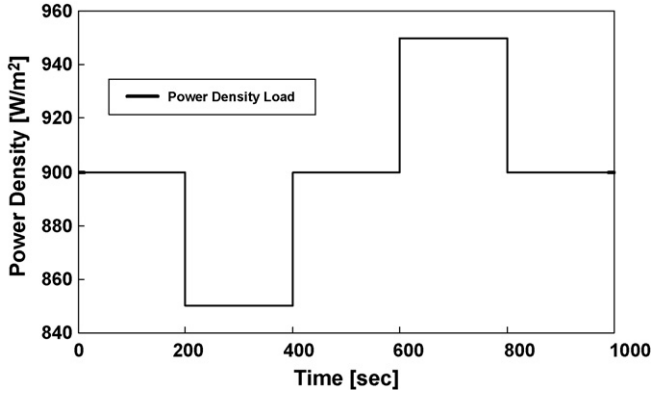

Fig. 15. Assumed power load in non-isothermal DMFC single-cell model.

Table 6
Initial guesses for decision variables in optimization

Variables	Initial guess value
Feed flow rate ($m^3\ s^{-1}$)	1.7×10^{-7}
Air flow rate ($m^3\ s^{-1}$)	2.0×10^{-5}
Feed concentration ($mol\ m^{-3}$)	1000

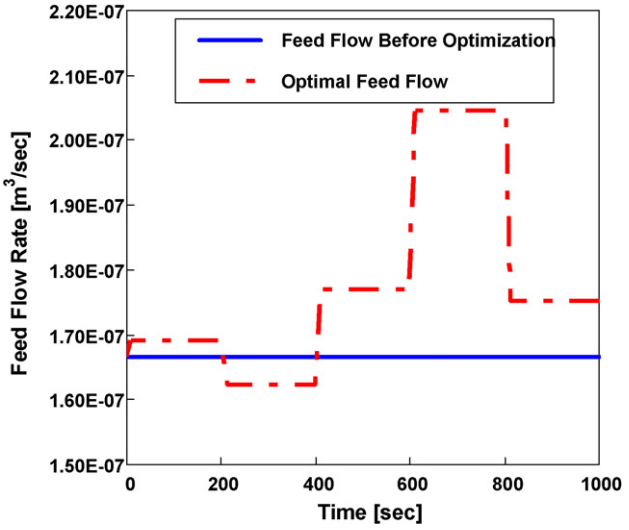

Fig. 16. Feed flow rate in non-isothermal DMFC model before and after optimization.

ables (flow rate of feed and air, and feed concentration) change proportionally to the power density load. That is the optimum values of the operating variables increase when the power load density increases. The optimum feed concentration is lower than the initial guess value because the methanol crossover is reduced with the low feed concentration and leads to high fuel efficiency. The optimum air flow rate increases compared with the value before the optimization, because a higher rate results in a higher voltage.

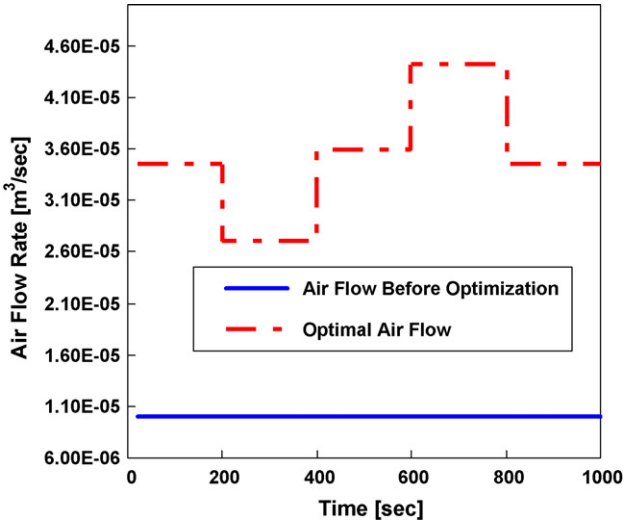

Fig. 17. Air flow rate in non-isothermal DMFC model before and after optimization.

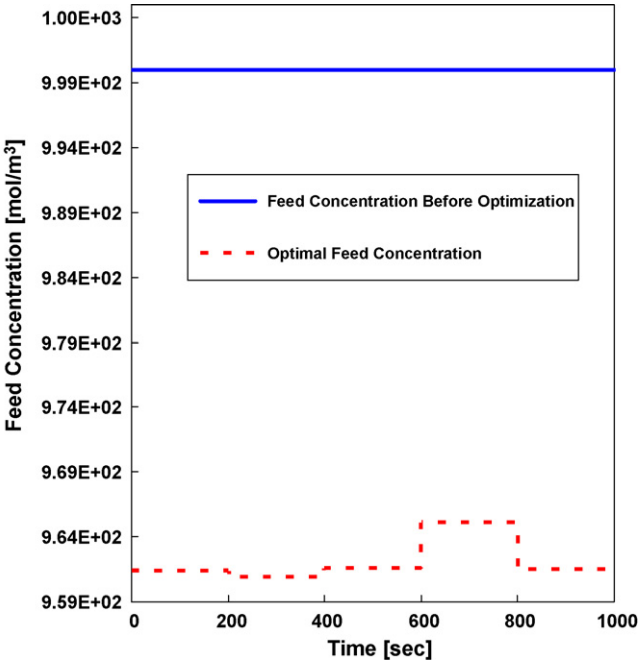

Fig. 18. Feed concentration in non-isothermal DMFC model before and after optimization.

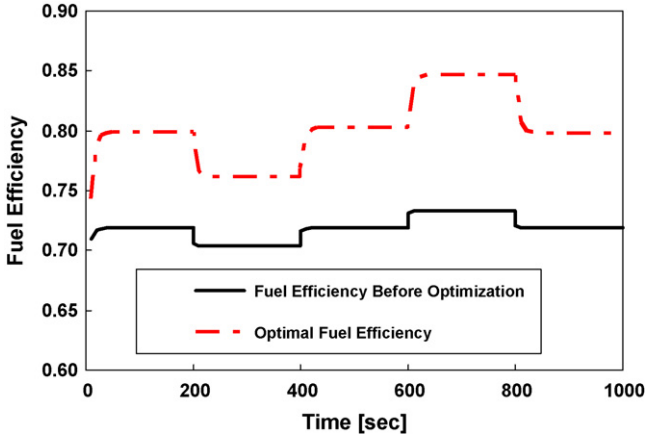

Fig. 19. Fuel efficiency before and after optimization (desired fuel efficiency = 0.80).

Judging from the results of the dynamic optimization and simulations, we find that methanol crossover is more affected by feed concentration than by the flow rates of the feed and air.

In this study, the optimum objective function value is 3.23×10^{-5} and the average fuel efficiency is 79.99%, which is extremely close to the desired fuel efficiency (=80%) as shown in the Fig. 19. Given these optimum conditions, the average fuel efficiency is enhanced from 71.78 to 79.99%. The total CPU time for the optimization is 1213.98 s on Pentium 4 with 3 GHz CPU and 512 MB RAM and the number of NLP iterations is 8.

5. Conclusions

A non-isothermal dynamic DMFC model is developed and incorporates electrochemical reaction kinetics and crossover

phenomena. This study is a foundation work to predict accurate stack temperature and dynamic behaviour for the efficient design of a DMFC stack and to find the optimum-operating conditions. For the further analysis and optimization of the non-isothermal dynamic fuel cell behaviour, reliable heat loss (convection, conduction, and radiation) needs to be considered within a non-adiabatic and non-isothermal model. Thus, an accurate temperature of a DMFC stack can be determined by including the exact heat loss calculation through an extended model. An accurate temperature prediction should be very helpful in reducing the cost of the optimum design and operation. The current basic model is adopted from the isothermal DMFC model of Sundmacher et al. [10] by adding the energy balance equation to predict the influence of temperature on the concentration loss of the cathode catalyst layer and on water crossover. To fit the non-isothermal DMFC MEA model to a practical MEA, model calibration through the optimization technique is carried out by estimating the chemical reaction constants (k_1, k_5, K_2, and K_4) and the parameters (B and $i_{\lim}$) of the cathode concentration loss term. The I–V and I–η_a points of the calibrated model show good agreement with the experimental data. The dynamic simulation and optimization of the calibrated model are carried out with a gPROMS modelling tool that includes the SRQPD algorithm for an optimization and a DASOLV code for a dynamic simulation. The present model describes the dynamic DMFC behaviour (voltage, crossover of methanol and water, temperature) successfully according to step changes of the operating variables (feed concentration, inlet flow rate into anode part, inlet flow rate into cathode part). The simulation results show that the feed concentration is a very important operating variable – because of its strong influence on the dynamic behaviour of the DMFC (temperature, crossover – voltage) compared with the flow rates of the feed and air. Also, the optimum-operating strategy can easily be established to achieve the desired fuel efficiency and to satisfy the varying power load through the dynamic optimization work. In conclusion, the simulation and optimization can efficiently provide an insight into the DMFC during dynamic operation and suggest optimum-operating strategies without the need for experimental data.

Acknowledgements

The authors are grateful to Dr. Heetak Kim and Dr. Junyoung Park at the fuel cell group of Samsung SDI for providing experimental data and helpful discussion on the modelling results.

Appendix A. Description of energy balance

The energy balance Eq. (13) consists of heat inlet and outlet, reaction heats, heat loss, and methanol oxidation heat resulting from the crossover. In this section, the equations included in the energy balance are described. The heat capacities of the cathode and the anode (C_{pc} and C_{pa}, respectively) are given by [21]:

$$\frac{C_{pc,i}}{R} = A_i + B_i T + C_i T^2 + D_i T^{-2} \tag{A1}$$

$$\frac{C_{pa,i}}{R} = A_i + B_i T + C_i T^2 + D_i T^{-2} \tag{A2}$$

where, the A_i, B_i, C_i, and D_i are the coefficients of heat capacity as listed in Table A1.

The reaction heats of the cathode and the anode ($Q_{c,rxn}$ and $Q_{a,rxn}$, respectively) are calculated by:

$$Q_{c,rxn} = \sum_i (h_{c,i}^{out} r_5 A^S) \tag{A3}$$

$$Q_{a,rxn} = \sum_i (h_{a,i}^{out} r_1 A^S) \tag{A4}$$

The enthalpies of the inlet and the outlet streams are given by [21].

$$\begin{aligned} h_{c,i}^{in} &= \int_{T_{ref}=298.15K}^{T_c^{in}} \left[R \left\{ \frac{C_{pc,i}}{R} \right\} \right] dT \\ &= \int_{T_{ref}=298.15\,K}^{T_c^{in}} [R\{A_i + B_i T + C_i T^2 + D_i T^{-2}\}] dT \\ &= H_{298,i}^{Cathode} + R \left[A_i + B_i \left(\frac{T_c^{in} + T_{ref}}{2} \right) \right. \\ &\quad \left. + \frac{C_i}{3} \{ (T_c^{in} + T_{ref})^2 - (T_c^{in} T_{ref}) \} + \frac{D_i}{(T_c^{in} T_{ref})} \right] \\ &\quad \times (T_c^{in} - T_{ref}) \end{aligned} \tag{A5}$$

Table A1
Coefficients of heat capacity for enthalpy calculations [20]

Component i		A	$B \times 10^3$	$C \times 10^6$	$D \times 10^{-5}$	Temperature range (K)
Anode						
CH_3OH	$i=1$	13.431	−51.28	131.13	0	273–373
H_2O	$i=2$	8.712	1.25	−0.18	0	273–373
CO_2	$i=3$	5.457	1.045	0	−1.157	298–2000
Cathode						
O_2	$i=1$	3.639	0.506	0	−0.227	298–2000
N_2	$i=2$	3.280	0.593	0	0.040	298–2000
H_2O	$i=3$	8.712	1.25	−0.18	0	273–373

$$h_{a,i}^{in} = \int_{T_{ref}=298.15\,K}^{T_a^{in}} \left[R\left\{ \frac{C_{pa,i}}{R} \right\} \right] dT$$
$$= \int_{T_{ref}=298.15\,K}^{T_a^{in}} [R\{A_i + B_i T + C_i T^2 + D_i T^{-2}\}] dT$$
$$= H_{298,i}^{Anode} + R\left[A_i + B_i \left(\frac{T_a^{in} + T_{ref}}{2} \right) + \frac{C_i}{3}\{(T_a^{in} + T_{ref})^2 - (T_a^{in} T_{ref})\} + \frac{D_i}{(T_a^{in} T_{ref})} \right] \times (T_a^{in} - T_{ref}) \quad (A6)$$

$$h_{c,i}^{out} = \int_{T_{ref}=298.15\,K}^{T_c^{out}} \left[R\left\{ \frac{C_{pc,i}}{R} \right\} \right] dT$$
$$= \int_{T_{ref}=298.15\,K}^{T_c^{out}} [R\{A_i + B_i T + C_i T^2 + D_i T^{-2}\} dT]$$
$$= H_{298,i}^{Cathode} + R\left[A_i + B_i \left(\frac{T_c^{out} + T_{ref}}{2} \right) + \frac{C_i}{3}\{(T_c^{out} + T_{ref})^2 - (T_c^{out} T_{ref})\} + \frac{D_i}{(T_c^{out} T_{ref})} \right] \times (T_c^{out} - T_{ref}) \quad (A7)$$

$$h_{a,i}^{out} = \int_{T_{ref}=298.15\,K}^{T_a^{out}} \left[R\left\{ \frac{C_{pa,i}}{R} \right\} \right] dT$$
$$= \int_{T_{ref}=298.15\,K}^{T_a^{out}} [R\{A_i + B_i T + C_i T^2 + D_i T^{-2}\}] dT$$
$$= H_{298,i}^{Anode} + R\left[A_i + B_i \left(\frac{T_a^{out} + T_{ref}}{2} \right) + \frac{C_i}{3}\{(T_a^{out} + T_{ref})^2 - (T_a^{out} T_{ref})\} + \frac{D_i}{(T_a^{out} T_{ref})} \right] \times (T_a^{out} - T_{ref}) \quad (A8)$$

Here, $T_{ref} = 298.15\,K$ and the values of the parameters (A_i, B_i, C_i, and D_i) are shown in Table A1.

The outlet temperatures from the cathode and the anode (T_c^{out} and T_a^{out}, respectively) are assumed to be the same as the cell temperature (T). T_c^{in} and T_a^{in} are the inlet temperatures into the cathode and the anode.

The methanol oxidation heat ($Q_{MeOHXover}$) is calculated by the Eq. (A9), and the methanol heat capacity ($C_{p,mh,MeOH\ Oxid}$) and total enthalpy change ($H_{298}^{Cell,total}$) by the Eqs. (A10) and (A11), respectively [21].

$$Q_{MeOHXover} = H_{298}^{Cell,total} + C_{p,mh,MeOH\ Oxid}(T - T_{ref}) \quad (A9)$$

Table A2
Joules per mole of substance formed at 298 K (standard heat of generation) [20]

Component i		$H_{298,i}$	State
Anode			
CH_3OH	$i=1$	−238,660	Liquid
H_2O	$i=2$	−285,830	Liquid
CO_2	$i=3$	−393,509	Gas
Cathode			
O_2	$i=1$	0	Gas
N_2	$i=2$	0	Gas
H_2O	$i=3$	−393,509	Liquid

$$\frac{C_{p,mh,MeOH\ Oxid}}{R} = 3.9915 + (55.584 \times 10^{-3})\left(\frac{T + 298.15}{2} \right) + \frac{(-131.49 \times 10^{-9})}{3}\{(T + 298.15)^2 - 298.15\,T\} + \frac{(-0.8165 \times 10^5)}{298.15\,T} \quad (A10)$$

$$H_{298}^{Cell,total} = H_{298}^{Anode,total} + H_{298}^{Cathode,total} \quad (A11)$$

$$H_{298}^{Anode,total} = H_{298,i=3}^{Anode} - H_{298,i=2}^{Anode} - H_{298,i=1}^{Anode} \quad (A12)$$

$$H_{298}^{Cathode,total} = 3H_{298,i=3}^{Cathode} - H_{298,i=2}^{Cathode} - 1.5H_{298,i} = 1^{Cathode} = 3H_{298,i=3}^{Cathode} \quad (A13)$$

Each value of $H_{298,i}$ is shown in Table A2.

References

[1] C.Y. Chen, P. Yang, J. Power Sources 123 (2003) 37–42.
[2] D. Kim, E.A. Cho, S.A. Hong, I.H. Oh, H.Y. Ha, J. Power Sources 130 (2004) 172–177.
[3] J. Liu, G. Sun, F. Zhao, G. Wang, G. Zhao, L. Chen, B. Yi, Q. Xin, J. Power Sources 133 (2004) 175–180.
[4] T. Shimizu, T. Momma, M. Mohamedi, T. Osaka, S. Sarangapani, J. Power Sources 137 (2004) 277–283.
[5] R. Chen, T.S. Zhao, J. Power Sources 152 (2005) 122–130.
[6] A. Simoglou, P. Argyropoulos, E.B. Martin, K. Scott, A.J. Morris, W.M. Taama, Chem. Eng. Sci. 56 (2001) 6761–6772.
[7] A. Simoglou, P. Argyropoulos, E.B. Martin, K. Scott, A.J. Morris, W.M. Taama, Chem. Eng. Sci. 56 (2001) 6773–6779.
[8] H. Dohle, J. Mergel, D. Stolten, J. Power Sources 111 (2002) 268–282.
[9] H. Dohle, K. Wippermann, J. Power Sources 135 (2004) 152–164.
[10] K. Sundmacher, T. Schultz, S. Zhou, K. Scott, M. Ginkel, E.D. Gilles, Chem. Eng. Sci. 56 (2001) 333–341.
[11] U. Krewer, A. Kamat, K. Sundmacher, J. Electroanal. Chem. 609 (2) (2007) 105–119.
[12] T. Schultz, K. Sundmacher, J. Membr. Sci. 276 (1–2) (2006) 272–285.
[13] C.H. Cheng, K. Fei, C.W. Hong, Comput. Chem. Eng. 31 (4) (2007) 247–257.
[14] E. Kjeang, J. Goldak, M.R. Golriz, J. Gu, D. James, K. Kordesch, Fuel Cells 5 (4) (2005) 486–498.
[15] C. Xu, P.M. Follmann, L.T. Biegler, M.S. Jhon, Comp. Chem. Eng. 29 (8) (2005) 1849–1860.
[16] X. Ren, S. Gottesfeld, J. Electrochem. Soc. 148 (1) (2001) A87–A93.

[17] G.Q. Lu, F.Q. Liu, C.Y. Wang, Electrochem. Solid-State Lett. 8 (1) (2005) A1–A4.
[18] J. Larminie, A. Dicks, Fuel Cell Systems Explained, John Wiley & Sons, Ltd., England, 2002, pp. 50–52.
[19] PSE Ltd. gPROMS Introductory User Guide, 2004.
[20] W.L. McCabe, J.C. Smith, P. Harriott, Unit Operations of Chemical Engineering, 5th ed., McGraw-Hill, New York, 1995, pp. 194–243.
[21] H. Rhee, C. Lee, Y. You, Chem. Eng. Thermodyn., 4th ed., HeeJungDang, Korea, 1992, pp. 102–129.